1-2022

Advanced Anti-Buckling Device Coupled with Real-Time Digital Image Correlation for Complex Cyclic Tension-Compression Testing of Lightweight Materials

Akshat Agha

Fadi Abu-Farha

Advanced Anti-Buckling Device Coupled with Real-Time Digital Image Correlation for Complex Cyclic Tension-Compression Testing of Lightweight Materials

Akshat Agha*[1], Fadi Abu-Farha[1]

ABSTRACT

In sheet metal forming and stamping operations, modeling the behavior of sheet metal alloys for springback prediction is known to be very challenging, not only because of the complex models needed to account for kinematic hardening (such as the Yoshida-Uemori Model) but more importantly because of the experimental limitations of our ability to perform the complex tests needed to calibrate such models. For instance, reliable monotonic uniaxial compression tests and then cyclic tension-followed-by-compression tests are essential for characterizing the response of the material under those loading conditions, providing quantitative evaluation of the Bauschinger Effect and tension/compression asymmetry in the material, and ultimately generate the right data to calibrate the constitutive model. This work tries to shed some light on this topic by introducing a new anti-buckling device that is particularly designed to enable accurate and repeatable compression and cyclic testing. The device exerts side loading on the sheet test sample to prevent it from buckling during testing under compression loading conditions. The device is designed to

[1]*FADI-AMT LLC, 48 Brookfield Oaks Dr. Suite D, Greenville, SC, 29607, USA*
* Corresponding Author. Tel +1 (336) 346 4213; E-mail: akshat@fadi-amt.com
https://orcid.org/0000-0001-9992-1114

address the limitations of other approaches and devices presented in the literature, and features control and monitoring of side forces, self-centering, and the ability to achieve large plastic compressive strains. More importantly, digital image correlation (DIC) is integrated with the anti-buckling device and testing load frame to provide accurate strain measurements. In this study, DIC was used in a real-time mode (unlike the typical post-deformation mode) to facilitate accurate load reversal during cyclic testing. For validation, the presented setup was used for testing two selected materials with practical applications in the automotive body sector: 6016-T4 aluminum and DP980 steel sheets. The results demonstrate how the developed setup and the integration with real-time DIC provide a robust and reliable means for generating high-quality curves for the different tests needed for the calibration of springback models.

KEYWORDS

Anti-buckling Device, Cyclic Testing, Tension-Compression Test, Springback, Yoshida-Uemori Model, Digital Image Correlation, Real-Time Strain Control,

Introduction

In recent years, the drive towards designing and manufacturing energy-efficient vehicles has propelled the automotive industry towards lightweighting with advanced materials, including high strength aluminum alloys and advanced high strength steels (AHSS) exhibiting high strength and ductility. However, several undesirable phenomena are associated with the forming of such materials; prominent and complex springback response is among the most critical of them. Springback magnitude is directly proportional to the ratio of flow stresses to Young's modulus;

this makes it typically high for such high strength materials. More importantly, the strong anisotropy of aluminum alloys and the multi-phase microstructures of AHSS result in tension/compression asymmetry, leading to complex springback behaviors, and therefore demanding the development of complex predictive models.

Several efforts in the literature tried to understand the springback behavior of sheet metal alloys. During stamping, materials are known to experience loading and unloading cycles, as well as switching between tension and compression loading cases. Cold working in a material increases its tensile yield strength but has a negative impact on the compressive yield strength due to the Bauschinger effect[1,2]. When the material is unloaded after being loaded plastically, the stress-strain response, particularly for high strength steels, is non-linear. Upon reloading, the material shows a nonlinear elastic response that is different from the unstrained material. The elastic modulus decreases with the increase in plastic strain; a phenomenon known as the modulus decay[3-5]. These complex phenomena make it more challenging to model the springback behavior of lightweight metals. Predictive springback models in the literature are generally dependent on four types of material response, and thus require four corresponding types of physical mechanical tests: (i) uniaxial tension tests, (ii) tension load-unload tests, (iii) uniaxial compression tests, and (iii) tension-compression cyclic tests.

There are notable works by Yoshida-Uemori[6-7], Ghaei[3], Lee[5], Li[8], and Chongthairungruang[9] on the modeling of springback using cyclic tension-compression (TC) and loading-unloading (LU) curves. The use of cyclic TC data and uniaxial tension loading-unloading (LU) data is not only limited to springback prediction but is also extended to other forming applications like single point incremental forming of sheet metals[10]. Although there have been improvements in the theoretical modeling, material characterization techniques still lag in terms of the ability to produce reliable

data, simply due to the complex nature of these tests. Various experimental techniques have been tried to determine the material properties of sheet metals along cyclic loading paths. It is still possible to measure small compressive strains on round specimens with appropriate length-to-diameter ratios[11]; however, large strains under in-plane compression testing of sheet metals are not easy to obtain due to material tendency to buckle under compressive loading. There have been various methods and devices proposed in the literature to suppress the out-of-plane buckling while testing. Yoshida et al.[12] tested a laminated specimen consisting of multiple sheet metal dogbone specimens bonded by an adhesive to overcome buckling in a single specimen. The study was performed on a mild steel (SPCC) and high strength steel (SPFC), and a maximum cyclic strain of ~8% was obtained. Yoshida et al. successfully used this approach to generate full-cycle tension-compression loops. While the results are encouraging, the approach may not be practical. Yoshida et al used a clip-on extensometer for strain measurements. Boger et al.[13] used solid flat plates as buckling constraints and applied normal side force on the test specimen using a hydraulic clamping system. The side force was controlled but not recorded. The setup was used successfully for compressive testing of pre-strained tension samples, achieving compressive recovery strains of ~18% for AA6022 and Mg AZ31B, but without using any extensometers due to setup limitations. Full loops of cyclic tests were done using optical extensometers but to a small cyclic strain of 2%. Kuwabara et al.[14] proposed a new setup where two comb-type dies were used to support the sheet specimen during testing, and thus prevent it from buckling. Compressive strains of up to ~6% were achieved in monotonic compression testing for both phosphor bronze and AA6016-T4 sheets. Cyclic testing was performed, however, the maximum strain limit in a single loop cyclic test was ~1.5%. While this approach produced good results for the two mentioned materials, the test specimen was still prone to buckle in between each pair of teeth of the die. No details were

provided regarding the method used for strain measurements. Li et al.[15], on the other hand, also proposed a setup with two comb-type dies to support the test specimen; However, the setup relied on eight bolts for changing the amount of side force exerted on the specimen. While this was an improvement over the work of Kuwabara et al, the side force was still not easy to control. Real-time side force was recorded for friction force corrections. Strain measurements were done using an optical non-contact extensometer; however, the latter was tracking test specimen deformation through two slotted holes in the clamping plate. Full single loop cyclic tension-compression testing was performed on B170P1 and DP590 steel sheets, and a maximum compressive strain of ~6% was achieved. Cao et al.[16] developed a double-wedge setup to provide side force and prevent buckling in the specimen, yet the side force was achieved by six screws and thus did not allow quantification nor control of the side force during testing. Moreover, two fins had to be extended from each test specimen to enable strain monitoring by a laser extensometer. The setup was used to test BH180, DP600 steel and AA6111-T4 sheets to achieve monotonic compressive strains up to ~10%; no full-loop cyclic tension/compression testing (single or multiple loops) was reported. Overall, the fixtures and devices presented in the literature show good features, but they were not comprehensive to cover all issues encountered in this type of complex testing. Except for the work of Boger et al, none of the devices had a reliable control over the side force. Majority of the works either use no extensometer, or a clip-on extensometer. The attempts with non-contact extensometers are limited to low compressive strains. Therefore, none of the presented systems uses easy and reliable strain measurement techniques, particularly capitalizing on the latest developments in non-contact strain measurements via digital image correlation (DIC). The latter is so critical as we have no information on the degree of uniformity of strains developed in the material specimen during testing, and only DIC can reveal that. Few efforts showed testing of

AHSS; none tested any AHSS of ~1.0 GPa tensile strength or higher. Finally, none show high-quality multi-loop tension-compression cyclic curves for a good array of materials.

In this effort, a novel anti-buckling device for controlled and reliable sheet specimen support is introduced; the device addresses most of the open issues encountered in monotonic compression testing as well as cyclic tension-compression testing. The device is capable of controlling and recording the side forces on the specimen throughout the test, for friction and biaxial corrections in the test results. The device has auto-alignment feature which can adapt to sheet specimens of any thickness. Moreover, the device is integrated with digital image correlation (DIC) for full-field strain measurements within the test specimen. The DIC is not used in the conventional post-deformation mode; rather, it records the strains on the surface of the specimen in real-time mode that provides direct feedback to the testing system to enable precise strain reversal. The paper first explains the details of the anti-buckling device, and its integration with DIC, highlighting the features incorporated in order to resolve the prominent issues in this field of testing. Two materials are then considered: AA6016-T4 and DP980 steel sheets; the materials represent high strength grades of aluminum and steel with important automotive body applications. The developed setup is used to test the two materials covering the uniaxial tension, tension load-unload, uniaxial compression, and cyclic tension-compression tests. Results are then presented highlighting the ability to obtain high-quality stress/strain curves for high strains and multiple cyclic loops (for accurate calibration of the most complex kinematic hardening springback models), as well as the enrichment brought about by DIC in revealing the levels of deformation homogeneity that can be expected from such tests.

Materials and Methods

TEST SETUP

The core of the developed setup is the anti-buckling device; designed to fit any quasi-static load frame. In this study, the device was fitted on a ZwickRoell Z020 electro-mechanical load frame, equipped with a 20kN load cell for axial load measurements. The anti-buckling device is shown in Figure 1, and it is simply a rigid cage structure containing a drive train featuring an air cylinder and a load cell, and two contact blocks (plates) that sandwich a test specimen within the gage region. When the air cylinder is engaged via an external flow valve, the two plates apply a firm side force that can be accurately controlled (by the amount of applied air pressure) and also monitored and corrected via the side load cell. In addition to that, the whole cage assembly can slide freely in the horizontal direction to allow self-centering of the device. The flexible nature of this mechanism allows for enough space to mount and remove the test specimen during setup while accommodating sheet specimens of practically any thickness during testing. The test specimen is mounted to the load frame via two custom grips that can withstand pulling and pushing forces up to ~20kN. To reduce the effects of friction induced by the anti-buckling contact blocks, a lubricant is used between them and the test specimen.
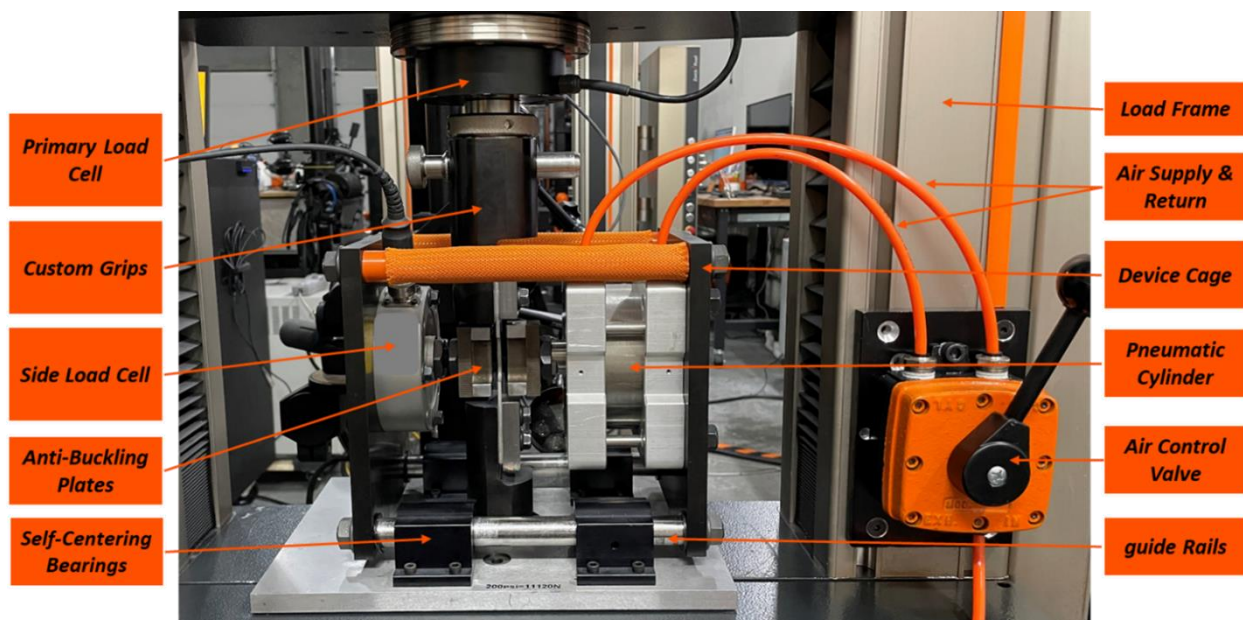
FIGURE 1. Anti-buckling device mounted onto a universal load frame.

Real-Time DIC System: The main highlight of the setup was the integration of 3D DIC with the anti-buckling device and the load frame. As shown in Figure 2, DIC cameras were set up for viewing the test specimen from the side (the free surface of the specimen since the gage region surfaces are under compression from the anti-buckling plates). The GOM ARAMIS 12M 3D DIC system with high-resolution cameras was used, achieving a measurement pixel density of less than 9microns per pixel. The specimens were speckle patterned on their sides, and the DIC system was set for tracking the axial strain along a 16mm long virtual extensometer. For the monotonic tension and compression tests, DIC was used in the conventional mode. For the cyclic tension-compression tests as well as the tension load-unload tests, the DIC system was operated in a real-time control mode and that is by feeding the live strains into the load frame; custom cyclic loading programs were prepared and the live DIC strains were used to accurately reverse the direction of loading at the exact points of interest.
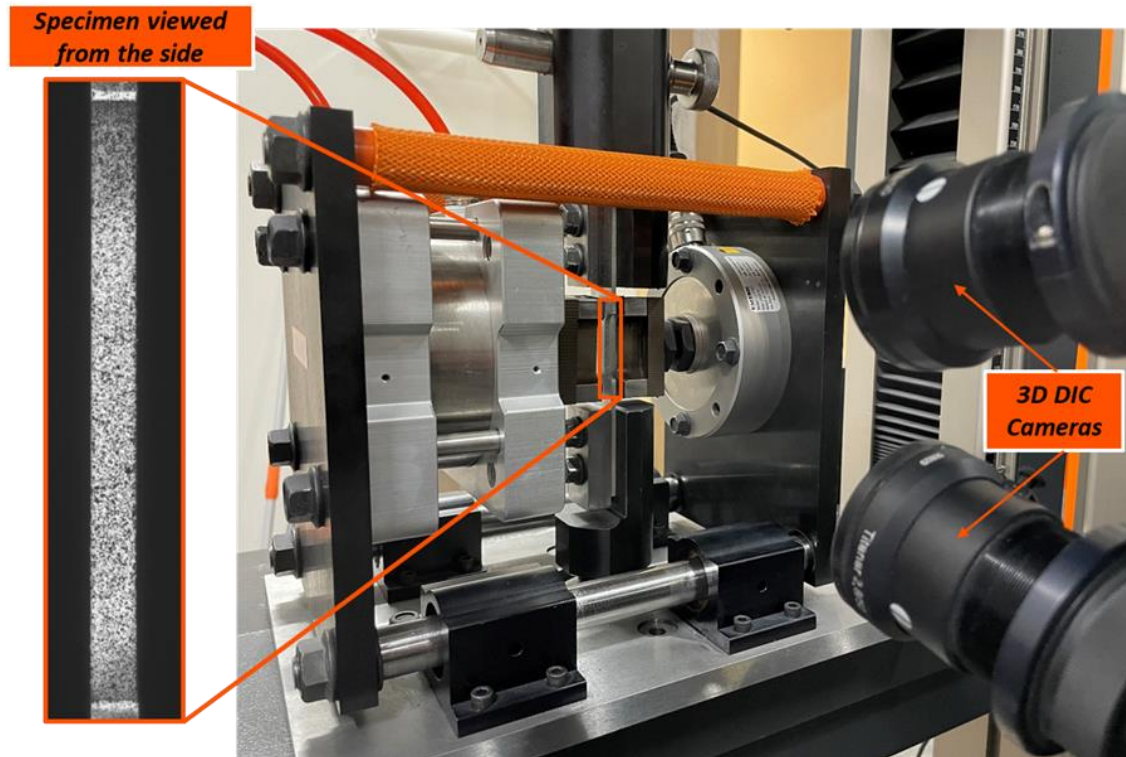
FIGURE 2. 3D DIC in real-time mode live tracking the deformation on the side of the specimen

MATERIALS

Two materials were selected for testing: 1.2mm thick DP980 steel sheets and 2.5mm thick AA6016-T4 sheets. The general relevant mechanical properties of these two materials are given in Table 1 below. Test specimens were cut out of the sheets by wire EDM per a custom geometry specifically suited for compression and cyclic testing; the same geometry was used for all tests including tension tests and load-unload tests to maintain consistency. The test specimens have a gage region of 20x10mm; while this is a low length-to-width ratio, it is necessary for this type of testing to assist in mitigating certain modes of buckling.

TABLE 1. Mechanical properties of the DP980 and AA6016-T4 sheets tested in this study

Material	Yield Strength (MPa)	Tensile Strength (MPa)	Total Ductility (%)
DP980	790	1056	16
AA6016-T4	165	275	32

Experimental Results and Analysis

TESTING CONDITIONS

All the mechanical tests performed in this study were carried out at an ambient temperature and a quasi-static strain rate of ~0.002 s^{-1} (axial pulling or compressive deformation). In the transverse direction, and for those tests that required the use of the anti-buckling device, a side force of 2kN was determined to be sufficient for the AA6016-T4 samples, while a higher side force of 4kN was used with the DP980 samples. DIC images were captured at a fixed frame rate of 20 Hz. Captured images were processed by GOM Correlate Professional DIC software.

UNIAXIAL TENSION TESTS

The uniaxial tension tests were first performed to establish the baseline behavior of each material. An Anti-buckling device is obviously not needed for tension testing; nevertheless, testing was carried out in two fashions: (i) without side force (anti-buckling plates fully open), and (ii) with side force from the anti-buckling device, and with the same level of forces used in subsequent compression and TC tests. The difference in force levels between the two scenarios was used to evaluate the friction forces from the contact blocks of the anti-buckling device, and that correction factor was used for correcting the forces during monotonic compression and cyclic TC tests. A comparison between the two tensile stress/strain curves, with and without side frictional forces, for both materials are shown in Figure 3. Note that the difference between them is small; the maximum deviation was determined to be ~1.8%.
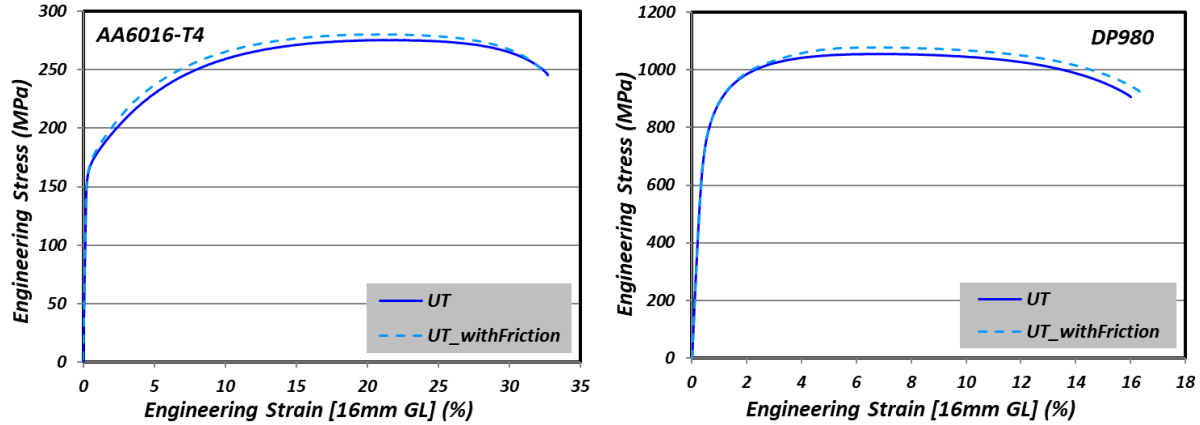
FIGURE 3. Stress/strain curves obtained by uniaxial tension testing with and without side force for (a) AA6016-T4 and (b) DP980

TENSION LOAD-UNLOAD TESTS

Though the tension load-unload tests do not require the anti-buckling device, they are included here to complete the suite of mechanical tests needed for a comprehensive calibration of constitutive models for springback prediction. This test is essential for evaluating the decay in Young's Modulus as a function of plastic strain. To maintain consistency, testing was still carried out with the same setup; the same specimen geometry and with the DIC cameras viewing the test specimen from the side. The test program was configured as a multi-loop cyclic tension test where each loading cycle is interrupted by unloading (to zero force) at a particular strain; then loading again and repeating the interruption to a greater strain. The interruption strain levels were selected to be 1%, 2%, 3%, 4%, 6% and 8% (as permitted by the material). The resulting stress/strain curves for both the AA6016-T4 and DP980 are shown in Figure 4. Greater disparity between the loading and unloading curves (higher deviation from linearity) is noted for the DP980, and the latter

increases with higher interruption strains. AA6016-T4 maintains a high level of elastic re-loading

curve linearity even at higher strains. Note that hints to the increasing non-linearity of the reloading

curves for DP980 compared to AA6016 can be inferred from the TC testing curves shown later.
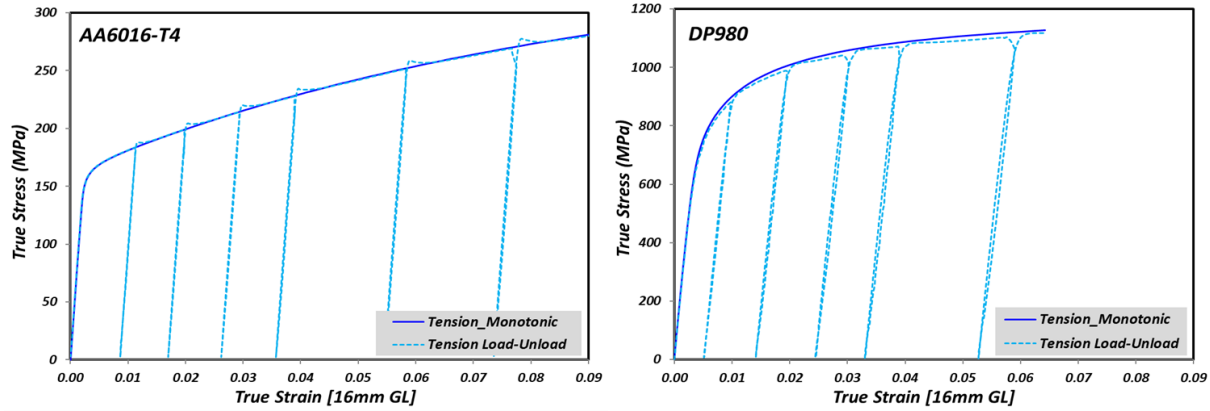

FIGURE 4. Plots showing stress-strain curve from uniaxial tension and uniaxial tension loading-

unloading tests for (a) AA6016-T4 and (b) DP980

By determining Young's Modulus for each loading cycle and plotting that against the plastic strain

level, the results shown in Figure 5 are obtained. A general exponential fit to capture the decay in

the modulus with plastic strain was presented in many efforts in the literature[12,17-19] ; the same

model was used here to extract the fitting trendlines shown also in Figure 5. Both materials show

notable decay that starts strong and progressively levels out. DP980 shows clear steady state

leveling with ~20% drop in Young's Modulus; most of this decay takes place after ~3% plastic

strain. AA6016-T4 exhibits a similar drop in Young's Modulus but after ~8% plastic strain, and

that is simply due to the much higher uniform tensile ductility (~25% for AA6016-T4 compared

to ~7% for DP980).

Though tension load-unload testing can be performed with conventional extensometry, the use of

DIC here brings the advantage of enabling the use of non-standard size samples (as is the case here) to match the geometry used for all the tests for springback characterization.
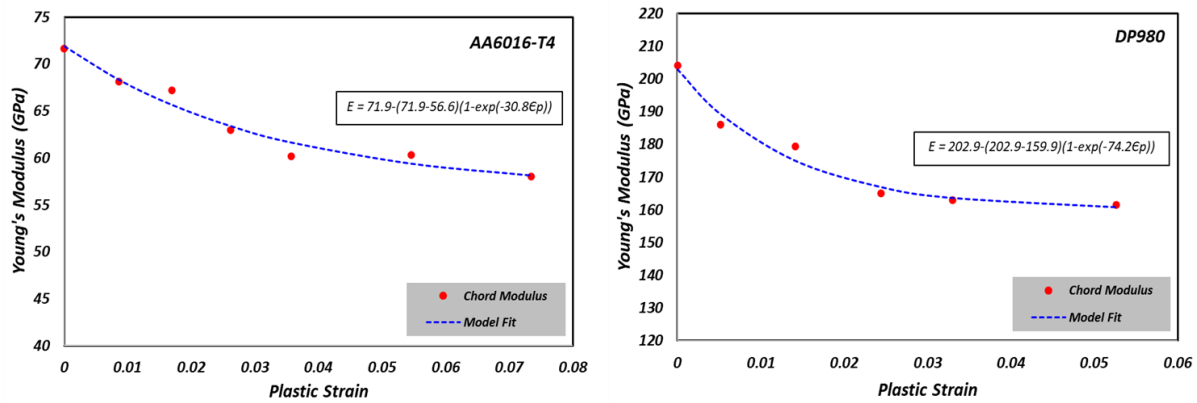

FIGURE 5. Plots of Young's Modulus decay with plastic strain for (a) AA6016-T4 and (b) DP980

UNIAXIAL COMPRESSION TESTS

Monotonic uniaxial compression tests were performed with the target of achieving plastic strains exceeding 10%. Tryout tests were first performed iteratively by trying increasing levels of side forces and observing the tested specimens for signs of buckling. 2kN and 4kN side forces were thus found to be satisfactory to prevent buckling in the AA6016-T4 and DP980 specimens, respectively. Actual testing then commenced, and the resulting stress/strain curves in comparison with those obtained from tension testing are shown in Figure 6. Note that the compression curves were intentionally flipped to the positive side of the plot to provide a direct comparison with the uniaxial tension stress/strain curves. As clearly seen, there is a notable difference in the stress level between tension and compression, indicating asymmetry in the properties of both materials. For AA6016-T4, this asymmetry is relatively modest and takes effect past the yield regime; in other

words, yield strength is almost the same for tension and compression, and asymmetry is mainly noted through a modest increase in the hardening exponent and post-yield flow stresses. For DP980, in addition to the higher compressive flow stress/strain curve, there is a relative rotation in the compressive curve around the yield regime when compared to the tension curve, which adds complexity to the asymmetric response of this material. Such behavior is mainly driven by the complex microstructures of AHSS (the different phases of ferrite, austenite, and martensite could have different tensile and compressive properties) and phase transformation with its dependency on the loading case (for austenite containing AHSS).

CYCLIC TENSION-COMPRESSION TESTS

The cyclic tension-compression tests (cycles of tension followed by compression tests) were performed over three loops with progressively higher plastic strain levels of 2.5%, 5%, and then 7.5%. In each loop, the test specimen is first stretched to the desired strain level before reversing the direction of loading to achieve the same limit in the compressive direction and then reversing to tension again to start the next loop. Three repeats of cyclic TC tests were performed for each material. The stress-strain curves for these cyclic tests were also plotted against the earlier monotonic tension and compression testing curves shown in Figure 6. The curves show good repeatability for the first TC loop, and then the curves slightly diverge in the second and third loop. This is due to the damage in the material with increasing strain accumulation over the TC cycles. These curves show clear differences between the two materials, particularly in the nature of their response to such cyclic loading. AA6016-T4 which showed a modest asymmetry between monotonic tension and compression shows a complex response to cyclic loading, simply characterized by a significant increase in the overall flow stress level after each cycle. DP980 on

the other hand shows no such increase; rather the three loops portray seamless progression as if any TC testing cycle to a particular strain level is simply a part of a bigger loop that represents the global response of the material. This does not make the response of DP980 any simpler as it exhibits early re-yielding for each new cycle, which is not the case with AA6016-T4 which shows a higher level of yielding stress for each new loading cycle! These great differences in the responses of the two materials demonstrate the importance of this particular test in revealing the complex behaviors of materials and thus enabling calibrating advanced springback constitutive models.
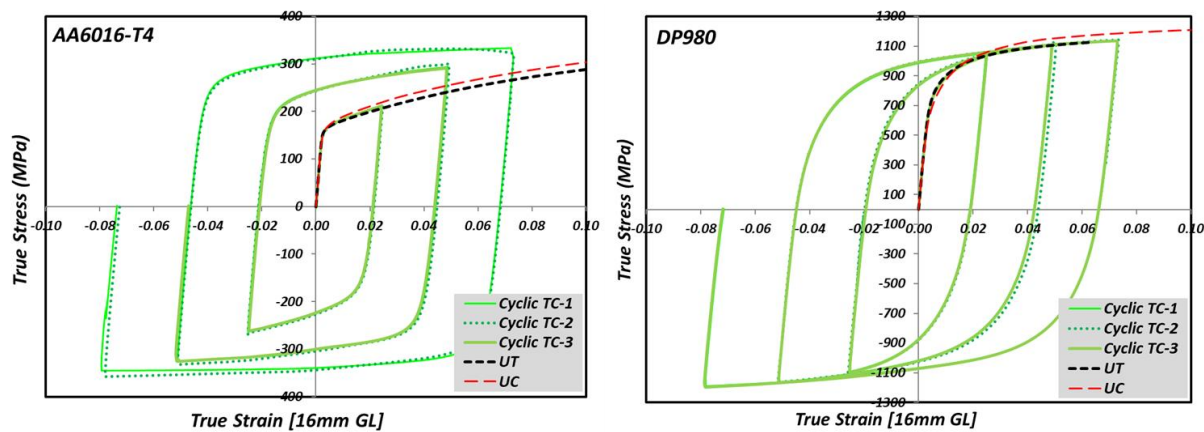

FIGURE 6. Stress-strain curves from monotonic tension tests, monotonic compression tests (flipped to positive), and 3 repeats of cyclic tension-compression tests for (a) AA6016-T4 and (b) DP980

A closer look at material deformation during cyclic testing was made possible with DIC by evaluating the homogeneity of plastic deformation across the test specimen at different strain levels. Figure 7 shows the full-field strain contour maps extracted for both materials at particular levels of plastic strains that correspond to the points of strain reversal. These maps reveal signs of deformation non-homogeneity as early as the first point of reversal; this non-homogeneity grows

stronger with additional plastic strain accumulations and strain reversals leading to the high levels at the end of each test. This is expected since the accumulative plastic strain imposed on the material during such cyclic tests is relatively high. When comparing the two materials, DP980 shows a greater level of non-homogeneity throughout the cyclic test, and that is also expected given its limited overall ductility (note that the uniform tensile ductility for this material is ~7%). These findings highlight the importance of using DIC in these tests as it provides a mechanism for determining the appropriate parameters of TC testing for a material based on its overall ductility.
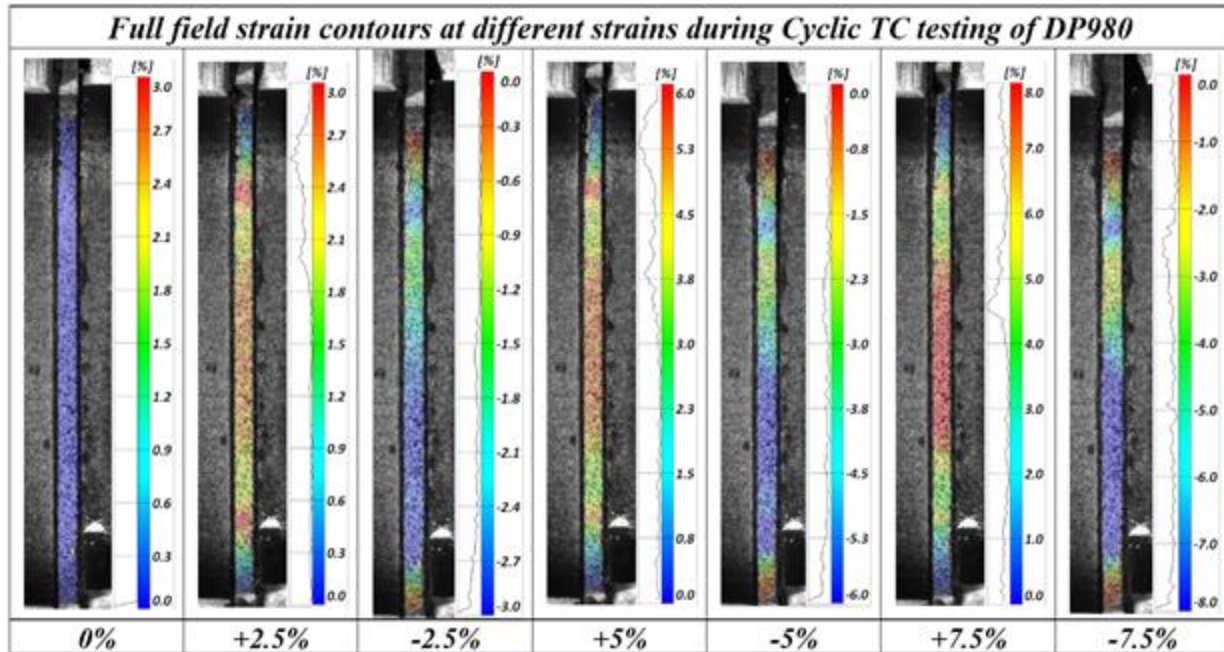

Full field strain contours at different strains during Cyclic TC testing of AA6016-T4
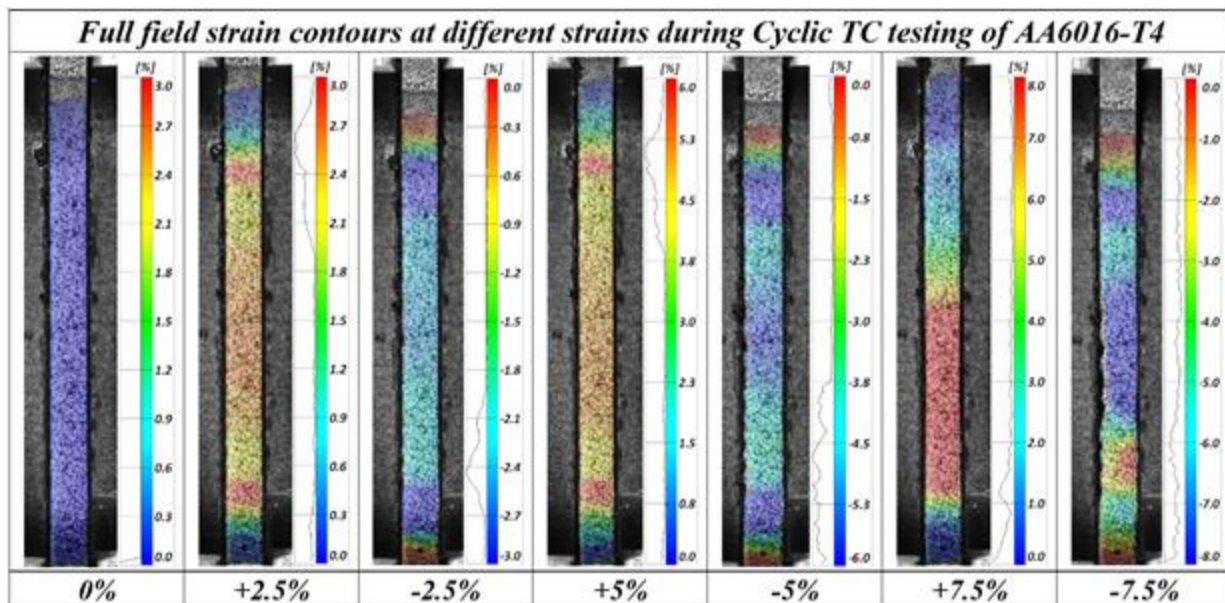
FIGURE 7. DIC generated strain maps extracted at particular points of interest (strains) during cyclic TC testing of (a) AA6016-T4 and (b) DP980 sheet samples

Conclusions

In this work, characterization and modeling of springback behavior in lightweight materials was addressed from an experimental point of view by presenting a novel anti-buckling device particularly designed for accurate and repeatable compression and cyclic testing; the two test types that are essential for calibrating complex spring constitutive models such as the Yoshida-Uemori Model[12]. In addition to the control and monitoring of side forces, self-centering, and the ability to achieve large plastic compressive strains, the anti-buckling device was coupled with digital image correlation (DIC) run in a unique real-time mode to enable accurate strain measurements and precise load reversal during cyclic testing. The integrated setup was validated by testing AA6016-

T4 aluminum and DP980 steel under different loading modes. It was shown how compression testing was successfully performed with both materials, developing compressive stress/strain curves reaching beyond 10%, and enabling good evaluation of tension/compression asymmetry in the materials. Cyclic tension-followed-by-compression tests were also successfully performed over several consecutive loops; the complexity of the test helped in revealing significant differences between the two materials in their response to alternating loading modes. In addition to the accurate strain measurements, DIC enriched these tests by revealing the levels of deformation non-homogeneities in the tested materials and their progression with plastic strain. While this paper does not offer answers as to why materials respond in different ways to complex compression or cyclic testing, as this is not the main objective in the first place, it simply offers the robust and reliable means for advanced characterization techniques to generate the data needed for calibrating complex springback predictive models.

References

1.   Weiss, M., et al., *On the Bauschinger effect in dual phase steel at high levels of strain.* Materials Science and Engineering: A, 2015. **643**: p. 127-136.
2.   Han, K., C.J. Van Tyne, and B.S. Levy, *Bauschinger Effect Response of Automotive Sheet Steels*. 2005, SAE International.
3.   Ghaei, A., D.E. Green, and A. Aryanpour, *Springback simulation of advanced high strength steels considering nonlinear elastic unloading–reloading behavior.* Materials & Design, 2015. **88**: p. 461-470.
4.   Mendiguren, J., et al., *Elastic behaviour characterisation of TRIP 700 steel by means of loading– unloading tests.* Materials Science and Engineering: A, 2015. **634**: p. 147-152.
5.   Lee, J.-Y., F. Barlat, and M.-G. Lee, *Constitutive and friction modeling for accurate springback analysis of advanced high strength steel sheets.* International Journal of Plasticity, 2015. **71**: p. 113-135.
6.   Yoshida, F. and T. Uemori, *A model of large-strain cyclic plasticity and its application to springback simulation.* International Journal of Mechanical Sciences, 2003. **45**(10): p. 1687-1702.
7.   Yoshida, F., T. Uemori, and S. Abe. *Modeling of large-strain cyclic plasticity for accurate springback simulation*. in *Key Engineering Materials*. 2007. Trans Tech Publ.

8.   Sun, L. and R.H. Wagoner, *Proportional and non-proportional hardening behavior of dual-phase steels.* International Journal of Plasticity, 2013. **45**: p. 174-187.
9.   Chongthairungruang, B., et al., *Experimental and numerical investigation of springback effect for advanced high strength dual phase steel.* Materials & Design, 2012. **39**: p. 318-328.
10.   Esmaeilpour, R., et al., *Effect of hardening law and process parameters on finite element simulation of single point incremental forming (SPIF) of 7075 aluminum alloy sheet.* Mechanics & Industry, 2020. **21**(3): p. 302.
11.   Zhou, F., Y. Chen, and Q. Wu, *Dependence of the cyclic response of structural steel on loading history under large inelastic strains.* Journal of Constructional Steel Research, 2015. **104**: p. 64-73.
12.   Fusahito Yoshida*, T.U., Kenji Fujiwara, *Elastic–plastic behavior of steel sheets under in-plane cyclic tension–compression at large strain.* International Journal of Plasticity, 2002. **18**: p. 633-659.
13.   Boger, R.K., et al., *Continuous, large strain, tension/compression testing of sheet material.* International Journal of Plasticity, 2005. **21**(12): p. 2319-2343.
14.   Kuwabara, T., et al., *Tension–compression asymmetry of phosphor bronze for electronic parts and its effect on bending behavior.* International Journal of Plasticity, 2009. **25**(9): p. 1759-1776.
15.   Qun Li, M.J., Zongyuan Zou*, Shiyan Zhao,Qingling Zhang, Peng Li, *Experiment Research on Tensile and Compression Cyclic Loading of Sheet Metal.* Procedia Engineering, 2017(207): p. 1916-1921.
16.   Cao, J., et al., *Experimental and numerical investigation of combined isotropic-kinematic hardening behavior of sheet metals.* International Journal of Plasticity, 2009. **25**(5): p. 942-972.
17.   Naofal, Naeini, and Mazdak, *Effects of Hardening Model and Variation of Elastic Modulus on Springback Prediction in Roll Forming.* Metals, 2019. **9**(9): p. 1005.
18.   Chen, Z., et al., *Variation and consistency of Young's modulus in steel.* Journal of Materials Processing Technology, 2016. **227**: p. 227-243.
19.   Chatti, S., *Modeling of the elastic modulus evolution in unloading-reloading stages.* International Journal of Material Forming, 2011. **6**(1): p. 93-101.